Ab Initio Calculation of Molecular Diffraction

Ab initio calculation of molecular diffraction

Thomas Northey, Nikola Zotev, and Adam Kirrander*

School of Chemistry, University of Edinburgh, West Mains Road, Edinburgh EH9 3JJ, United Kingdom

E-mail: Adam.Kirrander@ed.ac.uk
Phone: +44 (0)131 650 4716. Fax: +44 (0)131 650 6453

Abstract

We discuss the application of *ab initio* x-ray diffraction (AIXRD) to the interpretation of time-resolved and static x-ray diffraction. In our approach, elastic x-ray scattering is calculated directly from the *ab initio* multiconfigurational wave function via a Fourier transform of the electron density, using the first Born approximation for elastic scattering. Significant gains in efficiency can be obtained by performing the required Fourier transforms analytically, making it possible to combine the calculation of *ab initio* x-ray diffraction with expensive quantum dynamics simulations. We show that time-resolved x-ray diffraction can detect not only changes in molecular geometry, but also changes in the electronic state of a molecule. Calculations for cis-, trans-, and cyclo-butadiene, as well as benzene and 1,3-cyclohexadiene are included.

1 Introduction

Photochemical reactions have tremendous importance, ranging from photosynthesis to atmospheric chemistry, and technologies such as sensors and displays. They are intrinsically complex, with nonadiabatic dynamics[1] and conical intersections[2] known to play an important role, and they occur predominantly on the ultrashort time-scale.[3] For these and other reasons, a detailed understanding remains elusive.[4] However, new experimental techniques capable of monitoring photochemical processes in unprecedented detail are appearing.

Time-resolved x-ray diffraction imaging of atomic motion has already been demonstrated at third generation synchrotrons for comparatively slow molecular processes in condensed phases, such as photolysis[5,6] and vibrational relaxation[7] in solvents. Compared to time-resolved molecular spectroscopy, which ultimately measures energy levels and their populations, one major advantage of time-resolved structural dynamics is that it provides an immediate link to mechanistic chemistry. In principle structural dynamics, colloquially referred to as '*molecular movies*', can give direct access to molecular geometry as a function of time, including the spatial distributions of functional groups, steric hindrances, or spatial electrostatic charge distributions.

A new generation of x-ray sources known as x-ray free-electron lasers (XFELs)[8–12] have drastically advanced over the last 5 years. In 2009, the LCLS at Stanford became the first to successfully demonstrate free-electron lasing,[13] similarly followed in 2011 by SACLA in Japan.[14] New XFELs are under construction in Hamburg, Japan, Korea and Switzerland.[9,10,15,16] Their unprecedented pulse intensity allows for crystal-free diffraction imaging of biomolecules,[17–19] and the short duration and high intensity of the XFEL pulses means that ultrafast x-ray diffraction with spatial and temporal resolution is feasible.[20,21] Recently, diffraction from aligned[22,23] and unaligned[24] gas-phase molecules was demonstrated at the LCLS.

Since time-resolved x-ray diffraction is set to emerge as a powerful tool for structural dynamics and photochemistry, it is important to con-

*To whom correspondence should be addressed

nect the experiments with modern computational methods used for the analysis and interpretation of experiments.[25–27] We outline in this paper how the diffraction pattern of molecules can be calculated efficiently from multiconfigurational *ab initio* wave functions, connecting elastic x-ray scattering calculations with modern electronic structure methods. We examine the importance of the level of *ab initio* theory and the size of the basis set, and compare the *ab initio* x-ray diffraction patterns with those calculated by the independent atom model. We restrict ourselves to elastic x-ray scattering, and discussion of inelastic effects[28] is left for future publications.

An interesting question in the context of structural dynamics is if x-ray scattering can be used to identify the electronic state of a molecule.[29,30] Under specific conditions, x-ray diffraction from exceptionally long-lived electronic excited states in molecules has already been observed experimentally.[31–34] We show that even comparatively small changes in the electronic state of molecules are sufficient to leave signatures in the diffraction pattern, making it possible, at least in principle, to observe the changes in electronic state that accompany a chemical reaction.

2 Theory

2.1 Elastic x-ray scattering

The total x-ray scattering cross section for an N_{el}-electron system, according to Fermi's golden rule, can be written as,[35,36]

$$\frac{dI}{d\Omega} = \left(\frac{dI}{d\Omega}\right)_{Th} \sum_n \left(\frac{\omega_n}{\omega_0}\right) \left| \langle \Psi_n | \sum_{j=1}^{N_{\mathrm{el}}} e^{i\mathbf{q}\mathbf{r}_j} | \Psi_\alpha \rangle \right|^2 , \quad (1)$$

where $(dI/d\Omega)_{Th} = \left(e^2/mc^2\right) K$ is the Thomson cross section for an electron with m and e the electron mass and charge respectively, c the velocity of light, and K the polarization factor. Furthermore, ω_n and ω_0 are the frequencies of scattered and incident x-rays, and Ψ_n and Ψ_α are the wave functions of the nth final and the initial state. The elastic scattering term in Eq. (1), for $n = \alpha$, corresponds to the coherent scattering which plays a key role in x-ray structural determination.[37] This term

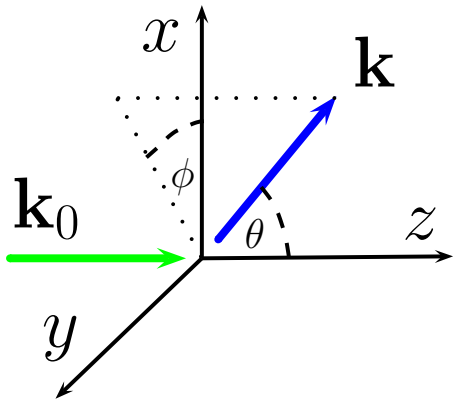

Figure 1: Schematic representation of the experimental geometry. The incoming wave vector $\mathbf{k}_0 = (0, 0, k_z)$ (in green) is aligned with the z-axis, and the scattered wave vector $\mathbf{k}(\theta, \phi)$ (in blue) is defined in terms of the radial, θ, and the azimuthal, ϕ, scattering angles, both defined relative to the direction of $\mathbf{k}_0$. The polarization direction of the excitation /alignment laser, when present, defines the x-axis.

is commonly expressed by the molecular form factor, $f^0(\mathbf{q})$, defined as

$$f^0(\mathbf{q}) = \langle \Psi_\alpha | \sum_{j=1}^{N_{\mathrm{el}}} e^{i\mathbf{q}\mathbf{r}_j} | \Psi_\alpha \rangle, \quad (2)$$

where the momentum transfer vector, $\mathbf{q}(\theta, \phi) = \mathbf{k}_0 - \mathbf{k}$, is defined as the difference between the incident and the scattered wave vectors, with $|\mathbf{k}| = |\mathbf{k}_0|$ for elastic scattering. The scattering angles θ (radial) and ϕ (azimuthal) give the direction of scattered radiation relative to the incoming x-ray, as shown in Fig. 1. For elastic scattering the amplitude of the scattering vector is $|\mathbf{q}| = 2|\mathbf{k}_0| \sin\theta/2$, i.e. it only depends on the radial scattering angle θ with values $0 \leq |\mathbf{q}| \leq 2|\mathbf{k}_0|$. Following Eq. (1), the intensity of the elastic kinematic diffraction from an atom or molecule is proportional to the square amplitude of the scattering form factor, $\left|f^0(\mathbf{q})\right|^2$.

The focus of this paper is the elastic scattering specific to a particular geometry and electronic state of the molecule, meaning that the scattering factor is taken to be instantaneous and therefore time-independent. The form factor in Eq. (2) can be shown to be the Fourier transform of the elec-

tron density,[37]

$$f^0(\mathbf{q};\bar{\mathbf{R}},\alpha) = \int \rho_{tot}^{(N_{\rm el})}(\mathbf{r};\bar{\mathbf{R}},\alpha)\, e^{\imath\mathbf{qr}} d\mathbf{r}, \qquad (3)$$

and it therefore depends parametrically on the electronic state α of the molecule, and on the $N_{\rm at}$ nuclear coordinates $\bar{\mathbf{R}} = (\mathbf{R}_1, \ldots, \mathbf{R}_{N_{\rm at}})$, with $\mathbf{R}_\gamma = (x_\gamma, y_\gamma, z_\gamma)$. The key quantity in Eq. (3) is the total electron density, $\rho_{tot}^{(N_{\rm el})}(\mathbf{r};\bar{\mathbf{R}},\alpha)$, with $N_{\rm el}$ the number of electrons. It is worth noting that $f^0(\mathbf{q}\equiv 0;\bar{\mathbf{R}},\alpha) = N_{\rm el}$ by definition. Approximate corrections for the inelastic scattering, per atom, have been calculated and tabulated using Waller-Hartree theory[38–40] and can be added to the coherent scattering.

In terms of time-dependent dynamics, the treatment embodied by Eq. (3) can be extended by calculating a *time-dependent* form factor, $f^0(\mathbf{q},t)$, that changes as the instantaneous electron density deforms. In doing this, it should be noted that when coherent quantum dynamics is probed by very short duration (large bandwidth) x-ray pulses, this approach produces incorrect results,[28,41,42] as recently demonstrated computationally for electronic wave packets in the hydrogen atom.[43] In brief, the large bandwidth makes it difficult to distinguish elastic from inelastic contribution to scattering. However, the time-dependent form factor approach remains applicable when the duration of the coherent x-ray pulses is short compared to the time-scale for nuclear motion, yet sufficiently long that the scattering cross-terms between different electronic states average out,[28,41,42] or when low-coherence x-ray sources are considered as in the case of time-resolved experiments at synchrotrons.[44]

A widespread approximation in both x-ray and electron diffraction, known as the independent atom model (IAM),[37] is to express the electron density as a sum of single-atom densities centered at each nuclear coordinate $\mathbf{R}_\gamma$ for a given molecular geometry. This results in the total form factor being a sum of atomic form factors,

$$f^{IAM}(\mathbf{q};\bar{\mathbf{R}}) = \sum_{\gamma=1}^{N_{\rm at}} f_\gamma^0(\mathbf{q}) e^{\imath\mathbf{qR}_\gamma}, \qquad (4)$$

where $f_\gamma^0(\mathbf{q})$ is the scattering form factor for each isolated atom γ in its ground state[40] and $\mathbf{R}_\gamma$ is the corresponding nuclear coordinate. The IAM approximation ignores the details of the electronic structure of the molecule, in particular the valence electrons responsible for chemical bonding.

In the present paper the form factor is determined analytically from the electron density via the *ab initio* wave function. We call this *ab initio* x-ray diffraction (AIXRD). Diffraction patterns calculated in this manner account for the specifics of each electronic state and the arrangement of the valence electrons, which ultimately is responsible for bonding and chemical reactivity. From the point of view of gas-phase experiments, we show that going beyond the IAM approximation is particularly valuable when a degree of spatial or rotational alignment is present.[23,45–48] We proceed by defining the *ab initio* electron density, then show how the required Fourier transform of the electron density can be calculated efficiently, and finally present the results for a number of different molecules. This extends previous work by Debnarova *et al.*[49] by deriving general analytic expressions for the Fourier transform of any Gaussian-type orbital, by examining the scattering from multiconfigurational wave functions, in particular in the context of excited states, and by investigating the relative merits, including computational efficiency and accuracy, of the IAM, the analytical AIXRD approach, and calculations using numerical FFT algorithms.

2.2 Electron density

In multiconfigurational *ab initio* theory the valence electrons are distributed over molecular orbitals in an active space which consists of electron configurations represented by Slater determinants. The multiconfigurational electronic state is therefore expanded as,

$$\Psi_\alpha = \sum_{i=1}^{N_{\rm conf}} c_{\alpha,i}\Phi_{SD}^i, \qquad (5)$$

where the $c_{\alpha,i}$ are the configuration interaction coefficients, $N_{\rm conf}$ is the number of configurations included in the expansion, and Φ_{SD}^i are the Slater

determinants for each configuration i, given by

$$\Phi^i_{SD} = \frac{1}{\sqrt{N!}} \sum_P (-1)^P P \Phi^i_H, \tag{6}$$

with P the pair-wise permutation operator acting on the Hartree product $\Phi^i_H = u^i_1(\mathbf{q}_1) \dots u^i_N(\mathbf{q}_N)$. The spin orbitals $u^i_j(\mathbf{q}_j)$ are the products of the spin functions $\chi(j)$ and the set of orthonormal spatial molecular orbitals, $\phi_j(\mathbf{r}_j)$, used to construct each Slater determinant.

The electron density is given by the operator,

$$\hat{\rho}(\mathbf{r}) = \sum_{j=1}^{N_{\rm el}} \delta(\mathbf{r} - \mathbf{r}_j), \tag{7}$$

which gives the total electron density as the sum of two components,

$$\begin{aligned} \rho^{(N_{\rm el})}_{tot}(\mathbf{r}; \bar{\mathbf{R}}, \alpha) &= \langle \Psi_\alpha | \hat{\rho} | \Psi_\alpha \rangle \\ &= \rho^{(N_{\rm el})}_{diag}(\mathbf{r}; \bar{\mathbf{R}}, \alpha) + \rho^{(0)}_{nd}(\mathbf{r}; \bar{\mathbf{R}}, \alpha). \end{aligned} \tag{8}$$

The diagonal component, $\rho^{(N_{\rm el})}_{diag}$, is a sum of the electron densities, $\rho^{(N_{\rm el})}_i$, for each of the Slater determinants,

$$\begin{aligned} \rho^{(N_{\rm el})}_{diag}(\mathbf{r}; \bar{\mathbf{R}}, \alpha) &= \sum_{i=1}^{N_{\rm conf}} c^2_{\alpha,i} \rho^{(N_{\rm el})}_i(\mathbf{r}; \bar{\mathbf{R}}, \alpha) \\ &= \sum_{i=1}^{N_{\rm conf}} c^2_{\alpha,i} \sum_{j=1}^{N_{\rm MO}} b^i_j \left|\phi_j(\mathbf{r})\right|^2 = \sum_{j=1}^{N_{\rm MO}} a_j |\phi_j(\mathbf{r})|^2, \end{aligned} \tag{9}$$

where the molecular orbitals have integer occupancies $b^i_j \in \{0, 1, 2\}$ that are different for each configuration. Partial occupancies for the $N_{\rm MO}$ molecular orbitals are $a_j = \sum_{i=1}^{N_{\rm conf}} c^2_{\alpha,i} b^i_j$. The nondiagonal component in Eq. (8), $\rho^{(0)}_{nd}$, corresponds to the cross-terms between different Slater determinants,

$$\rho^{(0)}_{nd}(\mathbf{r}; \bar{\mathbf{R}}, \alpha) = \sum_{i=1}^{N_{\rm conf}} \sum_{j=1}^{N_{\rm conf}} c_{\alpha,i} c_{\alpha,j} \rho^{(0)}_{ij}(\mathbf{r}; \bar{\mathbf{R}}, \alpha). \tag{10}$$

Since $\hat{\rho}(\mathbf{r})$ in Eq. (7) is an one-electron operator, the cross-terms $\rho^{(0)}_{ij}(\mathbf{r}; \bar{\mathbf{R}}, \alpha)$ in Eq. (10) are nonzero *only* when the two Slater determinants differ by one single spatial orbital, in which case they evaluate to,

$$\rho^{(0)}_{ij}(\mathbf{r}; \bar{\mathbf{R}}, \alpha) = \phi_{i'}(\mathbf{r}) \phi_{j'}(\mathbf{r}), \tag{11}$$

where i' and j' are the indices of the spatial orbitals that are different in the two configurations. Note that we assume that orbitals and coefficients are real-valued throughout, e.g. $c_{\alpha,i} = c^*_{\alpha,i}$ and $\phi_{i'} = \phi^*_{i'}$. The nondiagonal electron density $\rho^{(0)}_{nd}(\mathbf{r}; \bar{\mathbf{R}}, \alpha)$ does not contribute to the net electron density since the integral of $\rho^{(0)}_{nd}(\mathbf{r}; \bar{\mathbf{R}}, \alpha)$ is zero.

The basis set used to represent the spatial wave functions is of particular importance as Gaussian-type orbitals (GTOs) allow for many integrals, including the required Fourier integrals, to be calculated analytically. The molecular orbitals $\phi_j(\mathbf{r}_j)$ are obtained as linear combinations of the basis functions $G_k(\mathbf{r})$,

$$\phi_j(\mathbf{r}) = \sum_{k=1}^{N_{\rm BF}} \mathcal{M}^j_k G_k(\mathbf{r}), \tag{12}$$

where $\mathcal{M}^j_k$ are the molecular orbital expansion coefficients determined by solving the Schrödinger eigenvalue equation via the *ab initio* self-consistent field (SCF) procedure, and the total number of basis functions $G_k(\mathbf{r})$ is $N_{\rm BF}$, with $j \in N_{\rm MO} = N_{\rm BF}$. The density associated with each molecular orbital is therefore,

$$|\phi_j(\mathbf{r})|^2 = \sum_{k_1=1}^{N_{\rm BF}} \sum_{k_2=1}^{N_{\rm BF}} \mathcal{M}^j_{k_1} \mathcal{M}^j_{k_2} G_{k_1}(\mathbf{r}) G_{k_2}(\mathbf{r}), \tag{13}$$

with a very similar expression for the cross-terms in Eq. (11), except that the term $\mathcal{M}^j_{k_1} \mathcal{M}^j_{k_2}$ in Eq. (13) is replaced by $\mathcal{M}^{i'}_{k_1} \mathcal{M}^{j'}_{k_2}$. Each basis function $G_k(\mathbf{r})$, in turn, is a contraction of GTOs, $g_s(\mathbf{r})$, such that,

$$G_k(\mathbf{r}) = \sum_{s=1}^{n_k} \mu^k_s g^k_s(\mathbf{r}), \tag{14}$$

where μ^k_s are the basis set contraction coefficients for the primitive GTOs. The product $G_{k_1}(\mathbf{r}) G_{k_2}(\mathbf{r})$ in Eq. (13) becomes,

$$G_{k_1}(\mathbf{r}) G_{k_2}(\mathbf{r}) = \sum_{s_1=1}^{n_{k_1}} \sum_{s_2=1}^{n_{k_2}} \mu^{k_1}_{s_1} \mu^{k_2}_{s_2} g^{k_1}_{s_1}(\mathbf{r}) g^{k_2}_{s_2}(\mathbf{r}). \tag{15}$$

A Cartesian Gaussian-type orbital centered at co-

ordinates $\mathbf{r}_s = (x_s, y_s, z_s)$ has the form,

$$g_s(\mathbf{r}) = \mathcal{N}_s (x - x_s)^{l_s} (y - y_s)^{m_s} (z - z_s)^{n_s} e^{-\gamma_s (\mathbf{r} - \mathbf{r}_s)^2}, \tag{16}$$

with exponent γ_s, Cartesian orbital angular momentum $L_s = l_s + m_s + n_s$, and normalisation constant $\mathcal{N}_s$,

$$\mathcal{N}_s = \left(\frac{2}{\pi}\right)^{3/4} \frac{2^{(l_s+m_s+n_s)}\ \gamma_s^{(2l_s+2m_s+2n_s+3)/4}}{[(2l_s-1)!!(2m_s-1)!!(2n_s-1)!!]^{1/2}}. \tag{17}$$

Using the Gaussian product theorem[50] for the product $g^{k_1}_{s_1}(\mathbf{r}) g^{k_2}_{s_2}(\mathbf{r})$ in Eq. (15) we get,

$$g^{k_1}_{s_1}(\mathbf{r}) g^{k_2}_{s_2}(\mathbf{r}) = K^{k_1 k_2}_{s_1 s_2}\ g^{k_1 k_2}_{s_1 s_2}(\mathbf{r}), \tag{18}$$

where $K^{k_1 k_2}_{s_1 s_2} = \exp[-\gamma^{k_1}_{s_1} \gamma^{k_2}_{s_2} (\mathbf{r}^{k_1}_{s_1} - \mathbf{r}^{k_2}_{s_2})^2 / (\gamma^{k_1}_{s_1} + \gamma^{k_2}_{s_2})]$ and the new Gaussian, $g^{k_1 k_2}_{s_1 s_2}(\mathbf{r})$, has the exponent $\gamma^{k_1 k_2}_{s_1 s_2} = \gamma^{k_1}_{s_1} + \gamma^{k_2}_{s_2}$, and is centered at $\mathbf{r}^{k_1 k_2}_{s_1 s_2} = (\gamma^{k_1}_{s_1} \mathbf{r}^{k_1}_{s_1} + \gamma^{k_2}_{s_2} \mathbf{r}^{k_2}_{s_2}) / (\gamma^{k_1}_{s_1} + \gamma^{k_2}_{s_2})$. The final step is to combine the equations above to express the total electron density, $\rho^{(N_{\mathrm{el}})}_{tot}(\mathbf{r}; \bar{\mathbf{R}}, \alpha)$, as a sum over Gaussian functions that are products of GTOs. This is done in the next section.

2.3 Fourier Transforms

The scattering form factor in Eq. (3) is the Fourier transform of the total electron density as given by Eq. (8),

$$\begin{aligned} f^0(\mathbf{q}; \bar{\mathbf{R}}, \alpha) &= \mathcal{F}_{\mathbf{r}} \left[\rho^{(N_{\mathrm{el}})}_{tot}(\mathbf{r}; \bar{\mathbf{R}}, \alpha) \right] (\mathbf{q}) \\ &= f^0_{diag}(\mathbf{q}; \bar{\mathbf{R}}, \alpha) + f^0_{nd}(\mathbf{q}; \bar{\mathbf{R}}, \alpha). \end{aligned} \tag{19}$$

From Eqs. (9), (13), (15), and (18), the form factor f^0_{diag}, which corresponds to the diagonal electron density $\rho^{(N_{\mathrm{el}})}_{diag}$, is given as,

$$\begin{aligned} f^0_{diag}(\mathbf{s}; \bar{\mathbf{R}}, \alpha) \ = \ & \sum_{j=1}^{N_{\mathrm{MO}}} a_j \sum_{k_1, k_2}^{N_{\mathrm{BF}}} \mathcal{M}^j_{k_1} \mathcal{M}^j_{k_2} \sum_{s_1, s_2}^{\mathfrak{n}_{k_1}, \mathfrak{n}_{k_2}} \mu^{k_1}_{s_1} \mu^{k_2}_{s_2} K^{k_1 k_2}_{s_1 s_2} \\ & \times \ \mathcal{F}_{\mathbf{r}}[g^{k_1 k_2}_{s_1 s_2}(\mathbf{r})](\mathbf{q}). \end{aligned} \tag{20}$$

The form factor f^0_{nd}, corresponding to the nondiagonal density $\rho^{(0)}_{nd}$, is similarly obtained by using Eqs. (10) - (11) instead of Eq. (9),

$$\begin{aligned} f^0_{nd}(\mathbf{s}; \bar{\mathbf{R}}, \alpha) \ = \ & \sum_{i,j}^{N_{\mathrm{A}}} \delta_{ij}\, c_{\alpha,i} c_{\alpha,j} \sum_{k_1, k_2}^{N_{\mathrm{BF}}} \mathcal{M}^{i'}_{k_1} \mathcal{M}^{j'}_{k_2} \sum_{s_1, s_2}^{\mathfrak{n}_{k_1}, \mathfrak{n}_{k_2}} \mu^{k_1}_{s_1} \mu^{k_2}_{s_2} \\ & \times \ K^{k_1 k_2}_{s_1 s_2}\ \mathcal{F}_{\mathbf{r}}[g^{k_1 k_2}_{s_1 s_2}(\mathbf{r})](\mathbf{q}), \end{aligned} \tag{21}$$

where the delta function δ_{ij} is 1 when the two determinants i and j differ by one spatial orbital only.

Since the Cartesian coordinates (x, y, z) are linearly independent and each Gaussian function can be written as a product of x, y and z components,

$$g^{k_1 k_2}_{s_1 s_2}(\mathbf{r}) = \prod_{r'=x,y,z} g^{k_1 k_2}_{s_1 s_2}(r'), \tag{22}$$

the problem is reduced to the solution of one-dimensional Fourier transforms $\mathcal{F}_x \left[g^{k_1 k_2}_{s_1 s_2}(x) \right](q)$. These can be determined analytically, making computations efficient. The one-dimensional Gaussians to be Fourier transformed take the general form,

$$g(x; l) = x^l e^{-\gamma x^2}, \tag{23}$$

where l is the Cartesian angular momentum quantum number. Solutions for increasing values of l can be obtained recursively via the standard Fourier relation,

$$\mathcal{F}_x \left[x f(x) \right](q) = -\imath \frac{d}{dq} \mathcal{F}_x \left[f(x) \right](q). \tag{24}$$

Using Eq. (24) it is possible to derive a general formula for the Fourier transform of Eq. (23) as,

$$\mathcal{F}_x \left[g(x; l) \right](q) = \frac{\imath^l \sqrt{\pi} e^{-q^2/4\gamma}}{2^l \gamma^{(2l+1)/2}} \sum_{p=0}^{l/2} (-1)^p \frac{l! \gamma^p q^{l-2p}}{(l-2p)!\, p!}, \tag{25}$$

which is valid for any integer l such that $l \geq 0$. The Fourier transform for Gaussians centered at any arbitrary coordinate x_0 can be found using the standard Fourier shift relation $\mathcal{F}_x \left[f(x - x_0) \right](q) = \mathcal{F}_x \left[f(x) \right](q) \exp(\imath q x_0)$. Specific solutions for the Fourier transform of the product of two GTOs as they appear in Eq. (18) for cumulative values of $l = l_1 + l_2$ up to $l = 4$ are provided in Table 1.

Table 1: Fourier transforms of the product of two GTOs, $g_{12}(x;l_1,l_2) = (x-x_1)^{l_1}(x-x_2)^{l_2}e^{-\gamma_{12}(x-x_{12})^2}$, with $\gamma_{12} = \gamma_1+\gamma_2$ and $x_{12} = (\gamma_1 x_1+\gamma_2 x_2)/\gamma_{12}$. The factor a in the table is $a = (\imath q/2\gamma_{12}) + x_{12}$.

l_1 l_2	$\mathcal{F}_x[g_{12}(x;l_1,l_2)](q)$
0 0	$G_{00}(q) = \sqrt{\frac{\pi}{\gamma_{12}}}e^{-\frac{\gamma_1\gamma_2}{\gamma_{12}}(x_1-x_2)^2}e^{is_x x_{12}}e^{-s_x^2/4\gamma_{12}}$
1 0	$(a-x_1)\,G_{00}(q)$
2 0	$\left(a^2+\frac{1}{2\gamma_{12}}-2x_1a+x_1^2\right)G_{00}(q)$
1 1	$\left(a^2+\frac{1}{2\gamma_{12}}-(x_1+x_2)a+x_1x_2\right)G_{00}(q)$
3 0	$\left\{a^3-3x_1a^2+\left(3x_1^2+\frac{3}{2\gamma_{12}}\right)a -\frac{3x_1}{2\gamma_{12}}-x_1^3\right\}G_{00}(q)$
2 1	$\left\{a^3-(2x_1+x_2)a^2+\left(x_1^2+2x_1x_2 +\frac{3}{2\gamma_{12}}\right)a-\frac{2x_1+x_2}{2\gamma_{12}}-x_1^2x_2\right\}G_{00}(q)$
4 0	$\left\{a^4-4x_1a^3+\left(6x_1^2+\frac{3}{\gamma_{12}}\right)a^2 -\left(4x_1^3+\frac{6x_1}{\gamma_{12}}\right)a+\frac{3x_1^2}{\gamma_{12}}+x_1^4+\frac{3}{4\gamma_{12}^2}\right\}G_{00}(q)$
3 1	$\left\{a^4-(3x_1+x_2)a^3+3\left(x_1^2+x_1x_2 +\frac{1}{\gamma_{12}}\right)a^2-\left(x_1^3+3x_1^2x_2+\frac{9x_1+3x_2}{2\gamma_{12}}\right)a +\frac{3x_1x_2+3x_1^2}{2\gamma_{12}}+x_1^3x_2+\frac{3}{4\gamma_{12}^2}\right\}G_{00}(q)$
2 2	$\left\{a^4-2(x_1+x_2)a^3+\left(\frac{3}{\gamma_{12}}+x_1^2+x_2^2 +4x_1x_2\right)a^2-\left(2x_1^2x_2+2x_1x_2^2+\frac{3(x_1+x_2)}{\gamma_{12}}\right)a +\frac{x_1^2+x_2^2+4x_1x_2}{2\gamma_{12}}+x_1^2x_2^2+\frac{3}{4\gamma_{12}^2}\right\}G_{00}(q)$

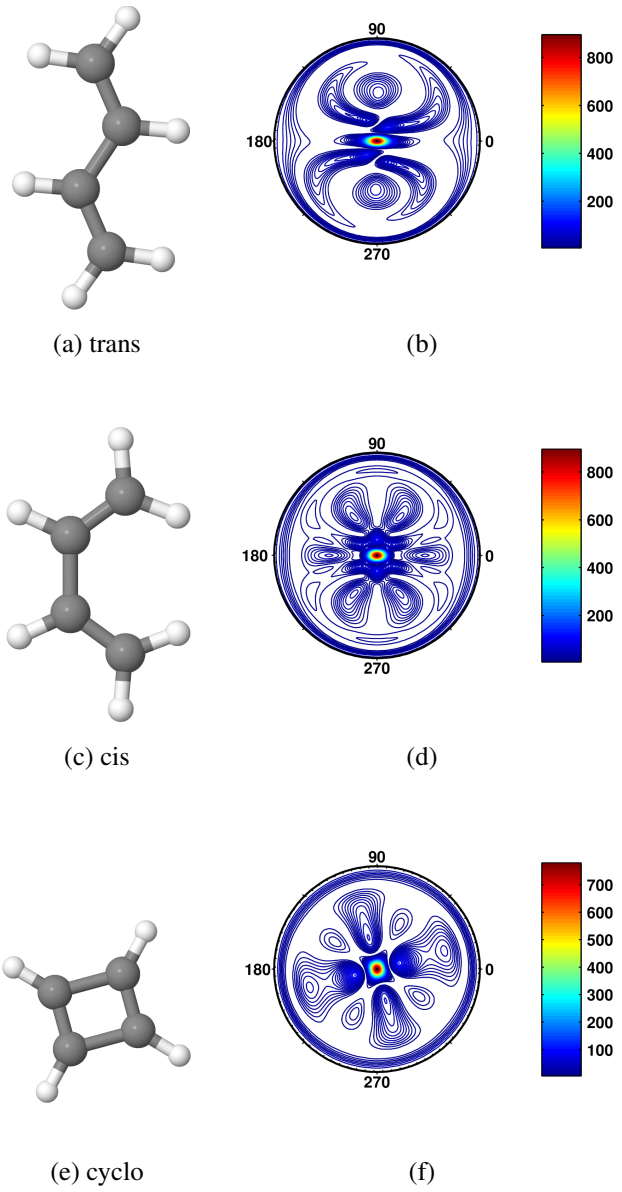

(a) trans (b)

(c) cis (d)

(e) cyclo (f)

Figure 2: Molecular geometry (left column) and x-ray diffraction (right column) for trans-, cis- and cyclo-butadiene. The diffraction, $|f^0(\mathbf{q};\bar{\mathbf{R}},\alpha)|^2$, shown in 2b, 2d and 2f is calculated for 1.3 Å x-rays using CASSCF *ab initio* wave functions obtained with the 6-31G(d,p) basis set. The scattering geometry is as shown in Fig. 1, with the molecules in the *xy*-plane. The scattering is given in terms of the radial angle θ (or equivalently the radius $|\mathbf{q}|$) and the azimuthal angle ϕ.

3 Results and Discussion

3.1 Molecular geometry, basis sets and the IAM

Structural dynamics,[24] or even static diffraction from aligned molecules,[23,45] is the most obvious target for new gas-phase x-ray diffraction experiments, since molecular geometry and changes in the molecular geometry leave strong signatures in the diffraction pattern. This is directly linked to the fact that each nucleus is strongly associated with a large number of electrons, in particular the core electrons, which track the motion of the nuclei closely. This is exploited in the independent atom model, where the diffraction *only* depends on the relative positions of the individual atoms. The effect of the molecular geometry on the diffraction pattern is illustrated by the trans and cis isomers of

butadiene, C_4H_6, shown in Figure 2. The molecular geometries and the associated diffraction patterns shown have been calculated using the complete active space self-consistent field (CASSCF) method[51] in MOLPRO[52] at the CASSCF(4,4)/6-31G(d,p) level, with 4 π-orbitals and 4 electrons in the active space. The energy of the geometry-optimized ground state is $E_{trans} = -154.985878$ a.u. for the trans and $E_{cis} = -154.980896$ a.u. for the cis isomer. The diffraction is calculated via Eq. (3) using Eq. (19), and is shown as $|f^0(\mathbf{q}; \bar{\mathbf{R}}, \alpha)|^2$. Here, and onwards, a x-ray wave length of 1.3 Å is assumed, meaning that the maximum value of scattering angle $\theta = \pi$ corresponds to $|\mathbf{q}| = 9.67$ Å^{-1}. As can be seen in Fig. 2, changes in geometry lead to significant changes in the diffraction, demonstrating the feasibility of tracking for instance the isomerization of butadiene by x-ray diffraction.

Figure 2 includes cyclo-butadiene, C_4H_4, calculated at the same level of theory with the energy of the geometry-optimized ground state $E_{cyclo} = -154.716941$ a.u.. The cyclo-butadiene is not square but in a rectangular geometry due to the Jahn-Teller effect.[53] Comparing the diffraction patterns for the three forms of butadiene shown in Fig. 2, it is evident that the point group of each molecule is reflected in the diffraction pattern. The molecular point groups are C_{2h}, C_{2v}, and D_{2h} for trans-, cis- and cyclo-butadiene. Overall, the diffraction patterns retain the same symmetry elements as that of the molecule, except that in the case of the diffraction pattern of cis-butadiene shown in Fig. 2d an extra inversion appears because mirror images of this molecule give the same diffraction pattern. It is well worth noting, though, that with limited alignment such point-group symmetries will be lost.

Since the molecular geometry exerts such a strong influence on the diffraction pattern, one may ask if it is worthwhile to go beyond the independent atom model. In Fig. 3a, the difference between the IAM diffraction calculated by Eq. (4) and the AIXRD (*ab initio* x-ray diffraction) calculated via Eq. (3) from the *ab initio* wave function, are shown for benzene. The geometry and electronic structure of the benzene molecule are calculated at the CASSCF(6,6)/6-31G(d,p) level of *ab initio* theory, with 6 π-orbitals and six electrons

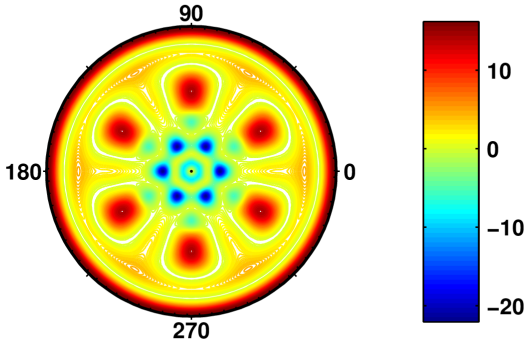

(a) Benzene diffraction: $|f_{6-31G(d,p)}|^2 - |f_{IAM}|^2$

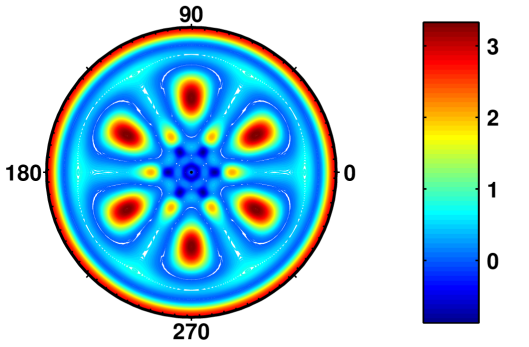

(b) Benzene diffraction: $|f_{6-31G(d,p)}|^2 - |f_{STO-3G}|^2|$

Figure 3: Comparison of diffraction patterns for benzene calculated at different levels of theory. (a) CASSCF(6,6)/6-31G(d,p) compared to the independent atom model (IAM), $|f_{6-31G(d,p)}|^2 - |f_{IAM}|^2$, with a 45% maximum difference. (b) CASSCF(6,6)/6-31G(d,p) compared to HF/STO-3G, $|f_{6-31G(d,p)}|^2 - |f_{STO-3G}|^2$, with a 9% maximum difference.

in the active space. The energy of the geometry-optimized ground state is $E_{benzene} = -230.786833$ a.u. and the C-C bond lengths are 1.396 Å. The maximum difference between the *ab initio* diffraction and the IAM is 45% in Fig. 3a. The differences are particularly pronounced in specific regions, corresponding to specific pixels on the detector in a would-be experiment. As mentioned earlier, the origin of the difference between the AIXRD and the IAM are the valence electrons in benzene.

Next, we examine the effect of the level of theory on the diffraction pattern. In Fig. 3b, the diffraction pattern calculated at the CASSCF(6,6)/6-31G(d,p) level (i.e. the same as in Fig. 3a) is compared to diffraction calculated from the corresponding Hartree-Fock (HF) STO-3G wave function. Here, the maximum difference is significantly smaller and amounts to approximately 9%. Since the computer time required for the diffraction calculations scales with the square of the number of Gaussian primitives (GTOs) included in the wave function, this means that HF/STO-3G constitutes a good compromise if computational speed is of the essence and the molecule is in the electronic ground state. In practice, the calculation of the diffraction pattern from a HF/STO-3G wave function is approximately four times faster than from the corresponding CASSCF(6,6)/6-31G(d,p) wave function. Multiconfigurational methods, such as configuration interaction (CI) or CASSCF, are computationally expensive and require larger basis sets than the minimal STO-3G to produce accurate results, but are necessary in order to calculate excited states accurately. Although AIXRD constitutes a significant improvement over IAM diffraction patterns already at comparatively low levels of *ab initio* theory, it is necessary to use high-level *ab initio* theory to accurately reproduce the diffraction from electronically excited molecules. The possibility of identifying the electronic state of molecules based on x-ray diffraction is discussed in the next section.

3.2 Electronic structure in diffraction

One strength of AIXRD is its ability to predict the diffraction pattern for excited states and individual molecular orbitals. The diffraction patterns for individual molecular orbitals, as demonstrated by σ and π^* molecular orbitals in O_2 and assuming single electron occupancy, are shown in Fig. 4. The orbitals are calculated for the optimised geometry at the CASSCF(8,8)/6-31G(d,p) level, with 4 π and 4 σ orbitals and 8 electrons in the active space, with the ground state energy at the optimized geometry $E_{O_2} = -149.663091$ a.u. and the bond length 1.245 Å. Characteristic diffraction patterns for each molecular orbital type (σ, σ^*, π, π^*) can be determined, and the appearance of diffuse orbitals or dominant bonds can be studied by x-ray diffraction combined with AIXRD.

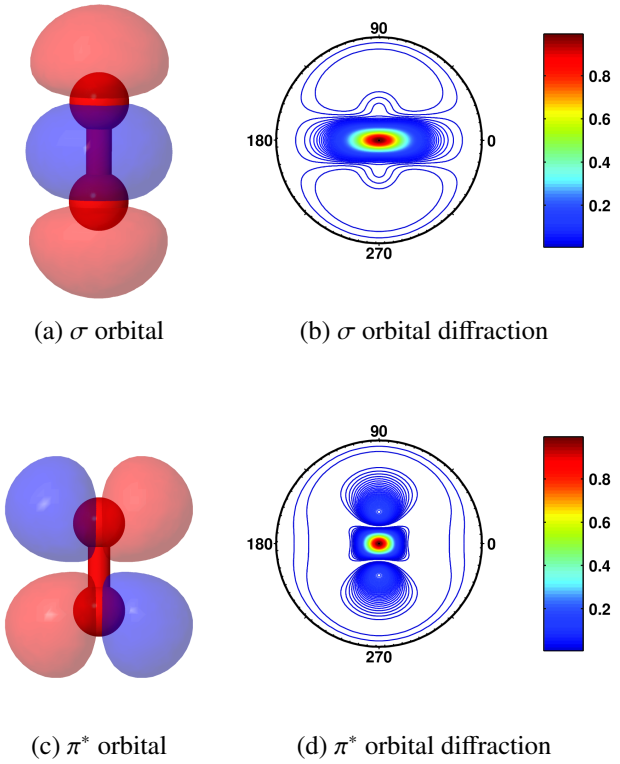

(a) σ orbital (b) σ orbital diffraction

(c) π^* orbital (d) π^* orbital diffraction

Figure 4: O_2 molecular orbitals (red and blue represent different phases) and their diffraction. (a) σ-bonding orbital, (b) σ orbital diffraction pattern, (c) π^*-antibonding orbital, and (d) π^* orbital diffraction pattern.

The more pertinent question is if it is possible to identify the electronic state of a molecule, or at least detect changes in the electronic state, by x-ray diffraction. The difficulty lies in the comparatively small number of valence electrons that change configuration during a transition between two electronic states, compared to the number of chemically inert electrons, which therefore dominate the diffraction signal. Especially during chemical reactions that are accompanied by structural changes, such as for instance a photochemical ring-opening or an isomerization reaction, it is non-trivial to distinguish the changes in the diffraction signal that are indicative of changes in the electronic configuration and those that are due to changes in geometry. Furthermore, experiments only excite a fraction of the molecules and there will always be a background of ground state molecules, which must be subtracted.[24,28]

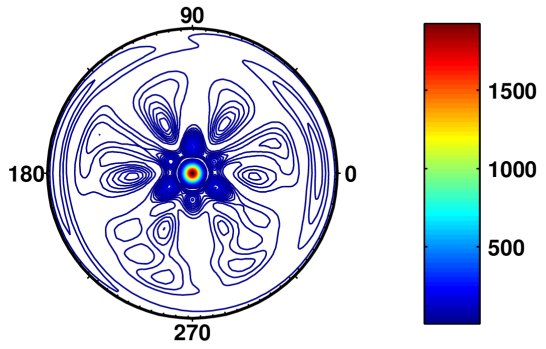

(a) Diffraction from the S_1 state of cyclohexadiene

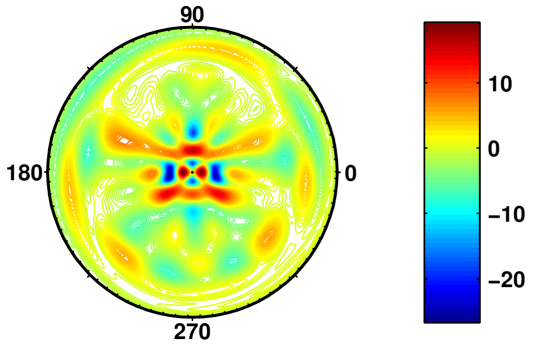

(b) Difference diffraction pattern for states S_1 and S_0

Figure 5: Diffraction from electronically excited states in 1,3-cyclohexadiene. (a) The diffraction pattern, $|f^0(\mathbf{q};\bar{\mathbf{R}}_0,S_1)|^2$, for the first singlet S_1 excited state in the ground state geometry. (b) The difference diffraction pattern, $|f^0(\mathbf{q};\bar{\mathbf{R}}_0,S_1)|^2 - |f^0(\mathbf{q};\bar{\mathbf{R}}_0,S_0)|^2$, between ground and first excited states. Red areas are characteristic of the excited state and blue areas of the electronic ground state.

Figure 5a shows the diffraction pattern of the first singlet excited state, S_1, of 1,3-cyclohexadiene obtained by vertical excitation from the ground state, S_0. The ground state geometry was optimised at the CASSCF(6,6)/6-31G(d,p) level of theory, with 4 π-orbitals and 4 π-electrons plus 2 σ-orbitals and 2 σ-electrons in the active space,[54] and then the ground and excited states were calculated at the optimized geometry. The ground and excited state energies at the optimized geometry are $E_{S_0} = -231.916756$ a.u. and $E_{S_1} = -231.668618$ a.u., respectively. Although the differences in the diffraction pattern between the ground and the first excited states, shown in Fig. 5b, are not large in absolute terms, they are nevertheless significant. The differences are particularly large in specific regions, shown in red or blue in Fig. 5b. In some pixels, the change in intensity, calculated as the ratio of $|f^0(S_0)|^2$ and $|f^0(S_1)|$, is up to 40%. Of course, the calculated diffraction patterns are calculated for static molecules, and in reality rotational and vibrational motion will blur the signal. However, sufficient differences to identify changes in the electronic state of the molecule may persist even once full rotational and vibrational averaging has been accounted for. Future work will take these considerations into account, but the results certainly highlight the value of alignment in gas-phase diffraction experiments.

3.3 Numerical calculations using FFT

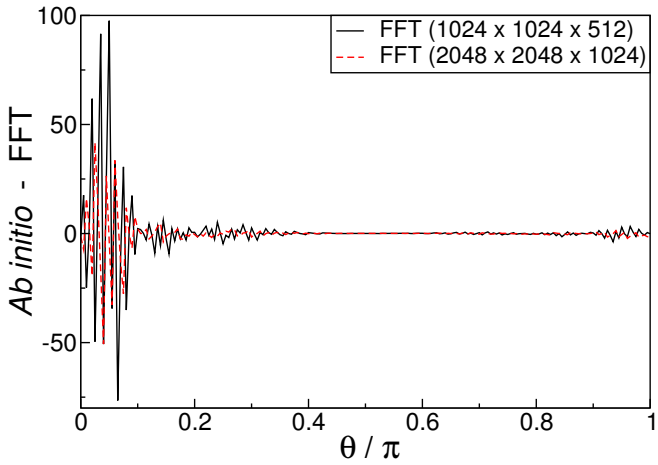

Figure 6: Convergence of numerical calculations using FFT. The difference between the diffraction calculated by numerical FFT and the *ab initio* analytical approach, $|f^0_{AIXRD}(\mathbf{q})|^2 - |f^0_{FFT}(\mathbf{q})|^2$, is shown. The comparison is made for the ground state benzene molecule as a function of the radial angle θ with azimuthal angle $\phi = 0$. The FFT has been calculated on two different size electron density grids, $1024 \times 1024 \times 512$ and $2048 \times 2048 \times 1024$. The error in the FFT calculation, relative the *ab initio* calculation, is on the order of 2.7% for the larger grid.

An alternative strategy to the analytic approach

to the calculation of elastic scattering discussed so far, is to represent the electron density in Eq. (8) on a spatial grid with regular spacing Δr and to Fourier transform the density numerically using a Fast Fourier Transform (FFT) algorithm.[55] This approach is conceptually simple and benefits from the numerical efficiency of FFT algorithms. However, as we will demonstrate, its utility depends on the accuracy of the results required.

In order to avoid problems with *aliasing*, which can severely degrade the accuracy of the FFT, one must ensure that the Fourier transformed signal is contained within the Nyquist critical frequency $q_c = 1/2\Delta r$, which is equivalent to saying that the the grid spacing Δr must be sufficiently small to adequately represent the molecular electron density. However, in many cases the Nyquist frequency is greater than $2|\mathbf{k}_0|$, meaning that to achieve the required resolution in the experimentally relevant region $0 \leq |\mathbf{q}| \leq 2|\mathbf{k}_0|$, a large total number of grid points must be used. This can be done by padding the electron density with trailing zeros, while ensuring that the resulting number of grid points, N_{grid}, in each spatial direction is a power of 2 for optimal performace of the FFT algorithm.[55] Since the three-dimensional FFT algorithm scales as $(N_{\text{grid}} \ln N_{\text{grid}})^3$, this quickly leads to significantly slower computations than might have been first anticipated. Additionally, there is a substantial overhead associated with the calculation of the electron density grid, a step which is bypassed in the analytic procedure since the Fourier transform is calculated directly from the wave function. A final advantage of the analytic approach is that we can choose exactly for which values of $\mathbf{q}$ to calculate the Fourier transform, and the transform is only computed for those required values.

Fig. 6 shows the convergence of the FFT to the analytic result for benzene, as a function of grid size. Due to the inherent periodicity of the discrete Fourier transforms, the FFT values deviate more from the correct values close to the edge regions. The addition of a very large number of trailing zeros should in principle resolve this issue, although at significant computational cost. The larger grid in Fig. 6 reproduces the analytic results with approximately 2.7% accuracy. The accuracy could be improved further by increasing the grid size, i.e. both the size of the electron density grid and the number of trailing zeros, but the numerical FFT calculations then become quite slow due to $(N_{\text{grid}} \ln N_{\text{grid}})^3$ scaling and the increasing overhead cost for calculating the electron density on the grid.

4 Conclusions

We have shown how the diffraction pattern for molecules can be calculated efficiently from *ab initio* multiconfigurational wave functions. We derive general analytical formulas for the Fourier transform of the electron density associated with any multiconfigurational wave function expressed in a Gaussian-type orbital basis. The use of analytic formulas bypasses the need to represent the electron density on a spatial grid followed by numeric Fourier transforms, leading to accurate and efficient calculations of elastic x-ray scattering.

The diffraction patterns calculated for isomers of butadiene demonstrate the potential of x-ray diffraction in tracking structural dynamics. We quantify the advantage of predicting x-ray diffraction patterns directly from *ab initio* wave functions (AIXRD) compared to the ubiquitous independent atom model (IAM), and show that accounting for the delocalized and bonding valence electrons makes up to a 45% difference in specific scattering directions for the benzene molecule. In very isotropic samples, such as a hot gas, and for structural dynamics that is confined to the ground electronic state, diffraction patterns predicted by IAM are likely to be sufficient. However, we show that IAM can be improved upon at modest computational expense by calculating AIXRD using basic electronic structure methods such as Hartree-Fock SCF with a small basis set. Such calculations already improve significantly on the results produced by IAM, and are particularly worthwhile when some degree of alignement or orientation is present in the sample.

For electronically excited states one must use multiconfigurational electronic structure methods to obtain reasonable accuracy in the excited state wave functions and energies. As these methods require larger-than-minimal basis sets to produce accurate results, the computational effort to calculate the diffraction patterns also increases. On

the upside, it is clear that, at least for molecules with a degree of rotational or spatial alignment, it should in principle be possible to detect signature changes in the diffraction pattern that correspond to transitions between electronic states, for instance during a photochemical reaction. At sufficient experimental resolution, one can even envision characterizing spectroscopic states based on diffraction.[30] Clearly, significant experimental challenges remain and the interpretation of the experimental data will be challenging, in particular in terms of separating out contributions from nuclear motion and changes in the electronic structure of the molecule.

With regards to computations, the conclusion is that we have a hierarchy of approaches. The independent atom model is the fastest by some margin, and gives adequate results in many situations. Results of intermediate quality are obtained most quickly by the numerical FFT approach. An advantage of the FFT approach is that it is not limited to Gaussian-type orbital basis sets, and can therefore straightforwardly be combined with e.g. plane-wave density functional theory calculations. The FFT approach holds a particular advantage over the analytical approach when fully rotationally averaged diffraction is required, as the rotational averaging can be done on the electron density grid, and then only a single one-dimensional FFT must be performed. The analytical approach is superior whenever high accuracy is required. For instance, capturing the comparatively small differences between ground and excited states with the numerical FFT approach would be challenging. In the context of time-dependent x-ray scattering, where the signals are quite weak in terms of the percent change in intensity, the added confidence from having accurate elastic cross-sections given by the analytic approach is valuable.

5 Future prospects

In future work, we plan to account for the full electronic and rotational-vibrational nuclear dynamics during a photochemical reaction, and determine the level of detail that is retained in the diffraction once the full averaging over nuclear and electronic degrees of freedom has been accounted for. We will also examine inelastic scattering effects, partially within the context of Fermi's Golden Rule via Waller-Hartree theory,[38] but also in the context of coherent dynamics probed by ultrashort coherent x-ray pulses.[41] One area of intense research at the new XFELs, such as the LCLS and the European XFEL, is crystal-free protein structure determination.[17–19] It is likely that such studies would benefit from *ab initio* diffraction patterns, along the lines presented in this paper, to interpret their diffraction data, and perhaps also by accounting for radiation damage explicitly.[56] Finally, one should note that the theory presented in this paper can easily be modified to account for elastic *electron* scattering, rather than x-ray scattering, by replacing the electron density in Eq. (19) (or equivalently Eq. (3)) with a charge density that includes the nuclear charges.[57–60]

Structural dynamics based on time-resolved elastic x-ray scattering has the potential to advance our experimental and theoretical understanding of how nuclei and electrons move during chemical reactions, and in particular our understanding of photochemical reactions, taking us towards the ultimate goal of *de novo* design of materials and molecules with specific optical, electric, photochemical or mechanical properties.

Acknowledgement The authors acknowledge funding from the European Union (FP7-PEOPLE-2013-CIG-NEWLIGHT) and helpful discussions with Dr. David Rogers at the University of Edinburgh regarding the *ab initio* electronic structure calculations.

References

(1) Worth, G. A.; Cederbaum, L. S. *Ann. Rev. Phys. Chem.* **2004**, *55*, 127.

(2) Domcke, W.; Yarkony, D. R. *Ann. Rev. Phys. Chem.* **2012**, *63*, 325.

(3) Zewail, A. H.; de Schryver, F. C.; Feyter, S. D.; Schweitzer, G. *Femtochemistry: with the Nobel lecture of A. Zewail*, 1st ed.; Wiley-VCH, 2001.

(4) Stolow, A. *Faraday Disc.* **2013**, *163*, 9.

(5) Neutze, R.; Wouts, R.; Techert, S.; Davidsson, J.; Kocsis, M.; Kirrander, A.; Schotte, F.; Wulff, M. *Phys. Rev. Lett.* **2001**, *87*, 195508.

(6) Kong, Q.; Lee, J. H.; Russo, M. L.; Kim, T. K.; Lorenc, M.; Cammarata, M.; Bratos, S.; Buslaps, T.; Honkimaki, V.; Ihee, H.; Wulff, M. *Acta Cryst. A* **2010**, *66*, 252.

(7) Lee, J. H.; Wulff, M.; Bratos, S.; Petersen, J.; Guerin, L.; Leicknam, J.-C.; Cammarata, M.; Kong, Q.; Kim, J.; Møller, K. B.; Ihee, H. *J. Am. Chem. Soc.* **2013**, *135*, 3255.

(8) Bostedt, C.; Bozek, J. D.; Bucksbaum, P. H.; Coffee, R. N.; Hastings, J. B.; Huang, Z.; Lee, R. W.; Schorb, S.; Corlett, J. N.; Denes, P.; Emma, P.; Falcone, R. W.; Schoenlein, R. W.; Doumy, G.; Kanter, E. P.; Kraessig, B.; Southworth, S.; Young, L.; Fang, L.; Hoener, M.; Berrah, N.; Roedig, C.; DiMauro, L. F. *J. Phys. B* **2013**, *46*, 164003.

(9) Feldhaus, J.; Krikunova, M.; Meyer, M.; Möller, T.; Moshammer, R.; Rudenko, A.; Tschentscher, T.; Ullrich, J. *J. Phys. B* **2013**, *46*, 164002.

(10) Yabashi, M.; Tanaka, H.; Tanaka, T.; Tomizawa, H.; Togashi, T.; Nagasono, M.; Ishikawa, T.; Harries, J. R.; Hikosaka, Y.; Hishikawa, A.; Nagaya, K.; Saito, N.; Shigemasa, E.; Yamanouchi, K.; Ueda, K. *J. Phys. B* **2013**, *46*, 164001.

(11) Lyamayev, V.; Ovcharenko, Y.; Katzy, R.; Devetta, M.; Bruder, L.; LaForge, A.; Mudrich, M.; Person, U.; Stienkemeier, F.; Krikunova, M.; Möller, T.; Piseri, P.; Avaldi, L.; Coreno, M.; O'Keeffe, P.; Bolognesi, P.; Alagia, M.; Kivimäki, A.; Fraia, M. D.; Brauer, N. B.; Drabbels, M.; Mazza, T.; Stranges, S.; Finetti, P.; Grazioli, C.; Plekan, O.; Richter, R.; Prince, K. C.; Callegari, C. *J. Phys. B* **2013**, *46*, 164007.

(12) Choi, J.; Huang, J. Y.; Kang, H. S.; Kim, M. G.; Yim, C. M.; Lee, T.-Y.; Oh, J. S.; Parc, Y. W.; Park, J. H.; Park, S. J.; Ko, I. S.; Kim, Y. J. *J. Korean Phys. Soc.* **2007**, *50*, 1372.

(13) Emma, P.; Akre, R.; Arthur, J.; Bionta, R.; Bostedt, C.; Bozek, J.; Brachmann, A.; Bucksbaum, P.; Coffee, R.; Decker, F.-J.; Ding, Y.; Dowell, D.; Edstrom, S.; Fisher, A.; Frisch, J.; Gilevich, S.; Hastings, J.; Hays, G.; Hering, P.; Huang, Z.; Iverson, R.; Loos, H.; Messerschmidt, M.; Miahnahri, A.; Moeller, S.; Nuhn, H.-D.; Pile, G.; Ratner, D.; Rzepiela, J.; Schultz, D.; Smith, T.; Stefan, P.; Tompkins, H.; Turner, J.; Welch, J.; White, W.; Wu, J.; Yocky, G.; Galayda, J. *Nat. Photon.* **2010**, *4*, 641.

(14) Ishikawa, T.; Aoyagi, H.; Asaka, T.; Asano, Y.; Azumi, N.; Bizen, T.; Ego, H.; Fukami, K.; Fukui, T.; Furukawa, Y.; Goto, S.; Hanaki, H.; Hara, T.; Hasegawa, T.; Hatsui, T.; Higashiya, A.; Hirono, T.; Hosoda, N.; Ishii, M.; Inagaki, T.; Inubushi, Y.; Itoga, T.; Joti, Y.; Kago, M.; Kameshima, T.; Kimura, H.; Kirihara, Y.; Kiyomichi, A.; Kobayashi, T.; Kondo, C.; Kudo, T.; Maesaka, H.; Maréchal, X. M.; Masuda, T.; Matsubara, S.; Matsumoto, T.; Matsushita, T.; Matsui, S.; Nagasono, M.; Nariyama, N.; Ohashi, H.; Ohata, T.; Ohshima, T.; Ono, S.; Otake, Y.; Saji, C.; Sakurai, T.; Sato, T.; Sawada, K.; Seike, T.; Shirasawa, K.; Sugimoto, T.; Suzuki, S.; Takahashi, S.; Takebe, H.; Takeshita, K.; Tamasaku, K.; Tanaka, H.; Tanaka, R.; Tanaka, T.; Togashi, T.; Togawa, K.; Tokuhisa, A.; Tomizawa, H.; Tono, K.; Wu, S.; Yabashi, M.; Yamaga, M.; Yamashita, A.; Yanagida, K.; Zhang, C.; Shintake, T.; Kitamura, H.; Kumagai, N. *Nat. Photon.* **2012**, *6*, 540.

(15) Kim, E.-S.; Yoon, M. *IEEE Trans. Nucl. Science* **2009**, *56*, 3597.

(16) Patterson, B. D.; Abela, R.; Braun, H.-H.; Flechsig, U.; Ganter, R.; Kim, Y.; Kirk, E.; Oppelt, A.; Pedrozzi, M.; Reiche, S.; Rivkin, L.; Schmidt, T.; Schmitt, B.; Strocov, V. N.; Tsujino, S.; Wrulich, A. F. *New J. Phys.* **2010**, *12*, 035012.

(17) Seibert, M. M.; Ekeberg, T.; Maia, F. R.

N. C.; Svenda, M.; Andreasson, J.; Jönsson, O.; Odic, D.; Iwan, B.; Rocker, A.; Westphal, D.; Hantke, M.; DePonte, D. P.; Barty, A.; Schulz, J.; Gumprecht, L.; Coppola, N.; Aquila, A.; Liang, M.; White, T. A.; Martin, A.; Caleman, C.; Stern, S.; Abergel, C.; Seltzer, V.; Claverie, J.-M.; Bostedt, C.; Bozek, J. D.; Boutet, S.; Miahnahri, A. A.; Messerschmidt, M.; Krzywinski, J.; Williams, G.; Hodgson, K. O.; Bogan, M. J.; Hampton, C. Y.; Sierra, R. G.; Starodub, D.; Andersson, I.; Bajt, S.; Barthelmess, M.; Spence, J. C. H.; Fromme, P.; Weierstall, U.; Kirian, R.; Hunter, M.; Doak, R. B.; Marchesini, S.; Hau-Riege, S. P.; Frank, M.; Shoeman, R. L.; Lomb, L.; Epp, S. W.; Hartmann, R.; Rolles, D.; Rudenko, A.; Schmidt, C.; Foucar, L.; Kimmel, N.; Holl, P.; Rudek, B.; Erk, B.; Hömke, A.; Reich, C.; Pietschner, D.; Weidenspointner, G.; Strüder, L.; Hauser, G.; Gorke, H.; Ullrich, J.; Schlichting, I.; Herrmann, S.; Schaller, G.; Schopper, F.; Soltau, H.; Kühnel, K.-U.; Andritschke, R.; Schröter, C.-D.; Krasniqi, F.; Bott, M.; Schorb, S.; Rupp, D.; Adolph, M.; Gorkhover, T.; Hirsemann, H.; Potdevin, G.; Graafsma, H.; Nilsson, B.; Chapman, H. N.; Hajdu, J. *Nature* **2011**, *470*, 78.

(18) Chapman, H. N.; Fromme, P.; Barty, A.; White, T. A.; Kirian, R. A.; Aquila, A.; Hunter, M. S.; Schulz, J.; DePonte, D. P.; Weierstall, U.; Doak, R. B.; Maia, F. R. N. C.; Martin, A. V.; Schlichting, I.; Lomb, L.; Coppola, N.; Shoeman, R. L.; Epp, S. W.; Hartmann, R.; Rolles, D.; Rudenko, A.; Foucar, L.; Kimmel, N.; Weidenspointner, G.; Holl, P.; Liang, M.; Barthelmess, M.; Caleman, C.; Boutet, S.; Bogan, M. J.; Krzywinski, J.; Bostedt, C.; Bajt, S.; Gumprecht, L.; Rudek, B.; Erk, B.; Schmidt, C.; Homke, A.; Reich, C.; Pietschner, D.; Struder, L.; Hauser, G.; Gorke, H.; Ullrich, J.; Herrmann, S.; Schaller, G.; Schopper, F.; Soltan, H.; Kuhne, K.-U.; Messerschmidt, M.; Bozek, J. D.; Hau-Riege, S. P.; Frank, M.; Hampton, C. Y.; Sierra, R. G.; Starodub, D.; Williams, G. J.; Hajdu, J.; Timneanu, N.; Seibert, M. M.; Andreasson, J.; Rocker, A.; Jonsson, O.; Svenda, M.; Stern, S.; Nass, K.; Andritschke, R.; Schroter, C.-D.; Krasniqi, F.; Bott, M.; Schmidt, K. E.; Wang, X.; Grotjohann, I.; Holton, J. M.; Barends, T. R. M.; Neutze, R.; Marchesini, S.; Fromme, R.; Schorb, S.; Rupp, D.; Adolph, M.; Gorkhover, T.; Andersson, I.; Hirsemann, H.; Potdevin, G.; Graafsma, H.; Nilsson, B.; Spence, J. C. H. *Nature* **2011**, *470*, 73.

(19) Barends, T. R. M.; Foucar, L.; Botha, S.; Doak, R. B.; Shoeman, R. L.; Nass, K.; Koglin, J. E.; Williams, G. J.; Boutet, S.; Messerschmidt, M.; Schlichting, I. *Nature* **2013**, *505*, 244.

(20) Clark, J. N.; Beitra, L.; Xiong, G.; Higginbotham, A.; Fritz, D. M.; Lemke, H. T.; Zhu, D.; Chollet, M.; Williams, G. J.; Messerschmidt, M.; Abbey, B.; Harder, R. J.; Korsunsky, A. M.; Wark, J. S.; Robinson, I. K. *Science* **2013**, *341*, 56.

(21) Gaffney, K. J.; Chapman, H. N. *Science* **2007**, *316*, 1444.

(22) Küpper, J.; Stern, S.; Holmegaard, L.; Filsinger, F.; Rouzee, A.; Rolles, D.; Rudenko, A.; Johnsson, P.; Martin, A. V.; Adolph, M.; Aquila, A.; Bajt, S.; Barty, A.; Bostedt, C.; Bozek, J.; Caleman, C.; Coffee, R.; Coppola, N.; Delmas, T.; Epp, S.; Erk, B.; Foucar, L.; Gorkhover, T.; Gumprecht, L.; Hartmann, A.; Hartmann, R.; Hauser, G.; Holl, P.; Hömke, A.; Kimmel, N.; Krasniqi, F.; Kühnel, K.-U.; Maurer, J.; Messerschmidt, M.; Mosshammer, R.; Reich, C.; Rudek, B.; Santra, R.; Schlichting, I.; Schmidt, C.; Schorb, S.; Schulz, J.; Soltau, H.; Strüder, L.; Thøgersen, J.; Vrakking, M. J. J.; Weidenspointner, G.; White, T. A.; Wunderer, C.; Meijer, G.; Ullrich, J.; Stapelfeldt, H.; Chapman, H. N. *arXiv pre-print 1307.4577* **2013**,

(23) Stern, S.; Holmegaard, L.; Filsinger, F.; Rouzeée, A.; Rudenko, A.; Johnsson, P.;

Martin, A. V.; Barty, A.; Bostedt, C.; Bozek, J.; Coffee, R.; Epp, S.; Erk, B.; Foucar, L.; Hartmann, R.; Kimmel, N.; Kuühnel, K.-U.; Maurer, J.; Messerschmidt, M.; Rudek, B.; Starodub, D.; Thøgersen, J.; Weidenspointner, G.; White, T. A.; Stapeldfeldt, H.; Rolles, D.; Chapman, H. N.; Küpper, J. *Farad. Disc.* **2014**, *171*.

(24) Minitti, M. P.; Budarz, J. M.; Kirrander, A.; Robinson, J.; Lane, T. J.; Ratner, D.; Saita, K.; Northey, T.; Stankus, B.; Cofer-Shabica, V.; Hastings, J.; Weber, P. M. *Farad. Disc.* **2014**, *171*.

(25) Ben-Nun, M.; Cao, J.; Wilson, K. R. *J. Phys. Chem. A* **1997**, *101*, 8743.

(26) Cao, J.; Wilson, K. R. *J. Phys. Chem. A* **1998**, *102*, 9523.

(27) Debnarova, A.; Techert, S.; Schmatz, S. *J. Chem. Phys.* **2010**, *133*, 124309.

(28) Møller, K. B.; Henriksen, N. E. *Struct. Bond.* **2012**, *142*, 185.

(29) Ben-Nun, M.; Martinez, T. J.; Weber, P. M.; Wilson, K. R. *Chem. Phys. Lett.* **1996**, *262*, 405.

(30) Kirrander, A. *J. Chem. Phys* **2012**, *137*, 154310.

(31) Pressprich, M. R.; White, M. A.; Coppens, P. *J. Am. Chem. Soc.* **1993**, *115*, 6444.

(32) Pressprich, M. R.; White, M. A.; Vekhter, Y.; Coppens, P. *J. Am. Chem. Soc.* **1994**, *116*, 5233.

(33) Kim, C. D.; Pillet, S.; Wu, G.; Fullagar, W. K.; Coppens, P. *Acta Cryst. A* **2002**, *58*, 133.

(34) Christensen, M.; Haldrup, K.; Bechgaard, K.; Feidenhans'l, R.; Kong, Q.; Cammarata, M.; Russo, M. L.; Wulff, M.; Harrit, N.; Nielsen, M. M. *J. Am. Chem. Soc.* **2009**, *131*, 502.

(35) James, R. *The Optical Principles of the Diffraction of X-Rays*, 6th ed.; G. Bell and Sons Ltd, London, 1962.

(36) Schulke, W. *Electron Dynamics by Inelastic X-Ray Scattering*, 1st ed.; Oxford Science Publications, 2007.

(37) McMorrow, D.; Als-Nielsen, J. *Elements of Modern X-Ray Physics*, 2nd ed.; Wiley-Blackwell, 2011.

(38) Waller, I.; Hartree, D. R. *Proc. R. Soc. Lond. Ser.-A* **1929**, *124*, 119.

(39) Chantler, C. T. *J. Phys. Chem. Ref. Data* **2000**, *29*, 597.

(40) *International Tables for Crystallography Volume C: Mathematical, physical and chemical tables*, 2006th ed.; Wiley, 2006.

(41) Henriksen, N. E.; Møller, K. B. *J. Phys. Chem. B* **2008**, *112*, 558.

(42) Lorenz, U.; Møller, K. B.; Henriksen, N. E. *Phys. Rev. A* **2010**, *81*, 023422.

(43) Dixit, G.; Vendrell, O.; Santra, R. *PNAS* **2012**, *109*, 11636.

(44) Bratos, S.; Mirloup, F.; Vuilleumier, R.; Wulff, M. *J. Chem. Phys.* **2002**, *116*, 10615.

(45) Küpper, J.; Stern, S.; Holmegaard, L.; Filsinger, F.; Rouzeée, A.; Rudenko, A.; Johnsson, P.; Martin, A. V.; Adolph, M.; Aquila, A.; Bajt, S.; Barty, A.; Bostedt, C.; Bozek, J.; Caleman, C.; Coffee, R.; Coppola, N.; Delmas, T.; Epp, S.; Erk, B.; Foucar, L.; Gorkhover, T.; Gumprecht, L.; Hartmann, A.; Hartmann, R.; Hauser, G.; Holl, P.; Hoömke, A.; Kimmel, N.; Krasniqi, F.; Kuühnel, K.-U.; Maurer, J.; Messerschmidt, M.; Moshammer, R.; Reich, C.; Rudek, B.; Santra, R.; Schlichting, I.; Schmidt, C.; Schorb, S.; Schulz, J.; Soltau, H.; Spence, J. C. H.; Starodub, D.; Struüder, L.; Thøgersen, J.; Vrakking, M. J. J.; Weidenspointner, G.; White, T. A.; Wunderer, C.; Meijer, G.; Ullrich, J.; Stapelfeldt, H.; Rolles, D.; Chapman, H. N. *Phys. Rev. Lett.* **2014**, *112*, 083002.

(46) Debnarova, A.; Techert, S.; Schmatz, S. *J. Chem. Phys.* **2011**, *134*, 054302.

(47) Kuthirummal, N.; Weber, P. M. *Chem. Phys. Lett.* **2003**, *378*, 647.

(48) Christopher, H.; Yang, J.; Centurion, M. *Phys. Rev. Lett.* **2012**, *109*, 133202.

(49) Debnarova, A.; Techert, S. **2006**, *125*, 224101.

(50) Szabo, A.; Ostlund, N. S. *Modern Quantum Chemistry: Introduction to Advanced Electronic Structure Theory*, 2nd ed.; Dover Publishing Inc., 1996.

(51) Roos, B. O. *Lect. Notes in Quant. Chem.* **1992**, *58*, 177.

(52) Werner, H.-J.; Knowles, P. J.; Knizia, G.; Manby, F. R.; Schütz, M. MOLPRO, version 2012.1, a package of ab initio programs.

(53) Snyder, L. C. *J. Chem. Phys.* **1960**, *33*, 619.

(54) Nenov, A.; Kölle, P.; Robb, M. A.; de Vivie-Riedle, R. *J. Org. Chem.* **2010**, *75*, 123.

(55) Press, W.; Vetterling, W.; Teukolsky, S.; Flannery, B. *Numerical Recipes in Fortran*, 2nd ed.; Cambridge University Press, 1992.

(56) Curwood, E. K.; Quiney, H. M.; Nugent, K. A. *Phys. Rev. A* **2013**, *87*, 053407.

(57) Zewail, A. H. *Science* **2010**, *328*, 187.

(58) Aseyev, S. A.; Weber, P. M.; Ischenko, A. A. *J. Anal. Sci. Meth. Instr.* **2013**, *03*, 30.

(59) Kohl, D. A.; Shipsey, E. J. *Z. Phys. D* **1992**, *24*, 39.

(60) Böwering, N.; Volkmer, M.; Meier, C.; Lieschke, J.; Dreier, R. *J. Molec. Struct.* **1995**, *348*, 49.

Graphical TOC Entry